Olesia Pashina, Albert Seredin, Giulia Crotti, Giuseppe Della Valle, Andrey Bogdanov, Mihail Petrov, Costantino De Angelis
Excitation of surface plasmon-polaritons through optically induced ultrafast transient gratings
Physical Review Applied 25, 014002, 2026.
DOI: 10.1103/8gm3-w8n5

Excitation of surface plasmon-polaritons through optically-induced ultrafast transient gratings

Olesia Pashina,[1,2] Albert Seredin,[2] Giulia Crotti,[3] Giuseppe Della Valle,[3]
Andrey Bogdanov,[2,4] Mihail Petrov,[2,*] and Costantino De Angelis[1]

[1] *University of Brescia, Brescia, Italy*
[2] *School of Physics and Engineering, ITMO University, St. Petersburg 197101, Russia*
[3] *Polytechnic University of Milan, Milan, Italy*
[4] *Qingdao Innovation and Development Centre, Harbin Engineering University, Qingdao, Shandong 266000, China*

Ultrafast excitation of non-equilibrium carriers under intense pulses offers unique opportunities for controlling the optical properties of semiconductor materials. In this work, we propose a scheme for ultrafast generation of surface plasmon polaritons (SPPs) via a transient metagrating formed under two interfering optical pump pulses in the semiconductor GaAs thin film. The grating can be formed due to modulation of the refractive index associated with the non-equilibrium carrier generation. The formed temporal grating structure enables the generation of SPP waves at the GaAs/Ag interface via weak probe pulse excitation. We propose a theoretical model describing non-equilibrium carriers formation and diffusion and their contribution to permittivity modulation via Drude and band-filling mechanisms. We predict that by tuning the parameters of the pump and probe one can reach the critical coupling regime and achieve efficient generation of SPP at the times scales of 0.1-1 ps.

I. INTRODUCTION

The recent progress in nonlinear all-dielectric nanophotonics [1–5] naturally stimulated active studies of all-optical modulation of semiconductor and dielectric nanostructures such as single scatterers [6, 7] and metasurfaces [8–16]. On this path, thermooptical effect, probably, shows the largest values of Kerr-type nonlinearity leading to efficient modulation of linear and nonlinear light scattering [17–21] and reaching bistability regimes [22–25], but the modulation time scales can not be shorter than nanoseconds [22, 26]. At the same time, non-equilibrium carrier generation results in optical modulation at much shorter time scales ranging from hundreds of femtoseconds to picoseconds [27].

The ultrafast nonlinearity driven by the non-equilibrium carriers has already been utilized for the Kerr-type self-induced modification of scattering of single semiconductor metaatoms [6, 7] and light reflection and transmission in metasurface structures [10, 11, 14, 16] including fast light modulation in anisotropic structures [15]. In addition to self-induced modulation of optical properties, ultra-strong all-optical modulation of all-dielectric metasurfaces was achieved in the pump-probe scheme [28–30] also with the help of formation of polaritonic condensates in novel excitonic materials [31, 32].

The streamline strategy underlying the ultrafast all-optical manipulation and control of light is based on semiconductor nanostructures, such as single nanoantennas and metasurfaces, with pronounced resonant properties [1, 3, 33]: indeed, resonances allow to concentrate fields on subwavelength scales, granting superior modulation efficiency in compact structures with respect to non-resonant systems, e.g., thin films. On the other hand, fabrication of nanometric components with optimal quality for applications still represents a challenge for the manufacturer. Moreover, in terms of reconfigurability of optical functionality, regardless of the physical mechanism exploited for the reconfiguration (being electrical, thermal or hot carrier based), nanostructured materials pose a further substantial issue, i.e. the addressability of their individual nanoelements.

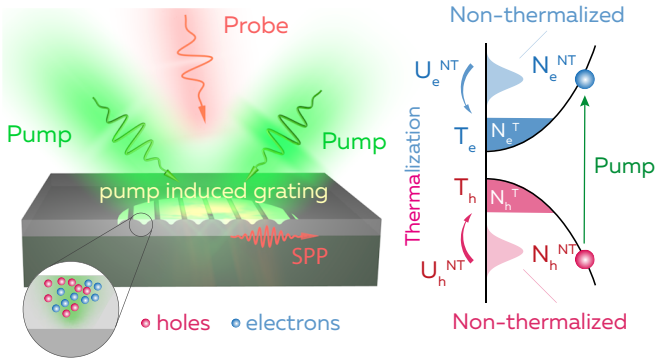

FIG. 1. Illustration of optically induced transient grating formation in GaAs film under the interference of pump fs-pulses with wavelength λ_{pump}. The grating is formed due to generation of non-equilibrium free-carriers under ultrashort pump excitation. Excitation of SPP wave at GaAs/Ag interface with probe pulse with wavelength λ_{pr}.

We present here a possible approach to tackle these limitations, based on the concept of spatial inhomogeneity in the photo-induced permittivity variation. We exploit the phenomenon of transient diffraction grating induced in a thin GaAs to excite surface plasmon-polaritons (SPPs) at the interface between the semiconductor thin film and a metallic medium. Such tran-

* m.petrov@metalab.ifmo.ru

sient diffraction gratings, formed through the interference of coherent light beams, are known to be crucial for investigating various semiconductor processes on nano- to femtosecond time scales. These gratings facilitate the study of dynamics related to thermal expansion[34], thermal [35] and ambipolar diffusion [36], surface recombination [37] , and other carrier relaxation phenomena [38, 39], as well as the crystallization of amorphous semiconductors [40] and carrier reaction kinetics [41]. Furthermore, they allow for the development of transient plasmonic metasurfaces in GaAs thin films, which offer tunable resonance conditions across a broad spectrum and enable functionalities such as perfect absorption [42]. The spatio-temporal grating formation in metals has also been explore recently [43–45]. Despite the notable progress in the realm of transient diffraction gratings, the ultrafast excitation and manipulation of surface plasmon polaritons through diffraction grating guidance remain largely unexplored, opening the possibility for a deeper understanding of semiconductor physics and paving the way for optically tunable ultrafast photonic devices.

The grating emergence is obtained with two crossed femtosecond pump pulses, whose interference grants a spatially periodic absorption pattern (see Fig. 1). In turn, this causes a periodic modulation of the permittivity $\Delta\varepsilon$ due to the non-equilibrium carriers' distribution: thus, the grating structure is transient, and exists at the time scale of carrier diffusion and recombination. In this ultrafast temporal window, SPPs can be excited at the GaAs/Ag interface with a probe pulse, as the diffraction grating allows to fulfill the necessary phase-matching condition [46].

To quantitatively discuss the key ideas presented above, we developed a theoretical description for the nonequilibrium carriers generation and transport dynamics at the nanoscale. Our self-consistent model represents a considerable expansion and improvement with respect to the approaches employed up-to-now to study the ultrafast response of semiconductor nanostructures, photoexcited with pulsed light.

II. RESULTS AND DISCUSSION

A. Theoretical model

Extended two-temperature model. Modeling of optically induced transient structures requires a comprehensive analysis of the generation, thermalization, diffusion, and recombination of free carriers, as well as their interaction with the lattice phonons. The most common approach is based on the extended two-temperature (eTT) model [43], which has already been actively used for describing ultrafast dynamics in metals [43] and metallic nanostructures [47]. Here we utilize eTT to model the dynamics of nonequilibrium processes occurring within a GaAs film when subjected to ultrashort laser pulse irradiation. Specifically, generation of nonequilibrium electron and hole charge carriers is caused by optically induced interband transitions. While the detailed description of the theoretical model is provided in Supplemental Information [48], Section 1, here we will present the key aspects of the model.

The formed non-thermalized carriers are described by the concentration $N_{\rm e}^{\rm NT}(\mathbf{r},t)$ and corresponding energy $\mathcal{U}_{\rm e}^{\rm NT}(\mathbf{r},t)$ as shown in Fig. 1. The Dember effect [58], which facilitates ambipolar diffusion of generated electrons and holes, enables us to assume that the evolution of charge carriers occurs in a nearly identical manner. Consequently, we can analyze our problem exclusively from the perspective of single charges, i.e. electrons. The subsequent carriers thermalization results in formation of their quasi-equilibrium distribution with temperature $T_e(\mathbf{r},t)$ and concentration $N_{\rm e}^{\rm T}(\mathbf{r},t)$. The further cooling of electron and hole subsystem due to interaction with phonons leads to increase of the lattice temperature $T_{ph}(\mathbf{r},t)$. The model also accounts for non-thermalized and thermalized carrier diffusion and relaxation, as well as for heat generation and diffusion. One can see the characteristic times of mentioned processes occurring in the structure in Table I.

The approach is based on the system of coupled differential equations describing the key characteristics dynamics with a spatiotemporal resolution (below each characteristic is assumed with $(\mathbf{r},t)$ dependence):

$$
\begin{aligned}
\frac{\partial \mathcal{U}_{\rm e}^{\rm NT}}{\partial t} &= \frac{1}{C_{\rm e}}\nabla\left[k_{\rm e}\nabla\mathcal{U}_{\rm e}^{\rm NT}\right] - \left(\Gamma_{\rm e}+\Gamma_{\rm ph}\right)\mathcal{U}_{\rm e}^{\rm NT} + Q_{\mathcal{U}_e},\\
\frac{\partial N_e^{\rm NT}}{\partial t} &= Q_{N_e} + \nabla\left[D\nabla N_e^{\rm NT}\right] - \Gamma_{\rm e}N_e^{\rm NT},\\
\frac{\partial N_e^{\rm T}}{\partial t} &= \Gamma_e N_e^{\rm NT} + \nabla\left[D\nabla N_e^{\rm T}\right] -\\
&\quad (\gamma_{nr}N_e^{\rm T} + \gamma_r {N_e^{\rm T}}^2 + \gamma_{Aug}{N_e^{\rm T}}^3),\\
\frac{\partial [C_e T_e]}{\partial t} &= \nabla\left[k_e\nabla T_e\right] - G_{\rm e-ph}[T_e - T_{ph}] + \Gamma_{\rm e}\mathcal{U}_{\rm e}^{\rm NT},\\
\frac{\partial [C_{ph} T_{ph}]}{\partial t} &= \nabla[k_{ph}\nabla T_{ph}] + G_{\rm e-ph}[T_e - T_{ph}] + \Gamma_{\rm ph}\mathcal{U}_{\rm e}^{\rm NT},
\end{aligned}
\tag{1}
$$

Here Q_{N_e} and $Q_{\mathcal{U}_e}$ represent the concentration and energy sources characterized by optical absorption at each point of the structure defined by the imaginary part of the dielectric permittivity $\varepsilon(\mathbf{r},t)$. The coefficients $C_{e/ph}$, $k_{e/ph}$, $\mu_{e/ph}$ correspond to the electron/phonon heat capacity, thermal conductivity, and mobility [59–61], respectively. Additionally, Γ_e denotes the rate of energy exchange between non-thermal and thermal electrons [62], while Γ_{ph} is the rate of energy transfer between electrons and phonons [43]. The electron-phonon relaxation time is given by $G_{\rm e-ph}$ [43, 63], and D is the coefficient for ambipolar heat diffusion [64]. It is worth noting that, in submicron semiconductor systems, ballistic transport [65] of hot carriers may become non-negligible. As discussed in the Supplementary Information [48] (Sec.

1E), the estimated Knudsen number indicates that the carrier mean free path can approach the characteristic size of the structure. In the present work, however, we restrict our analysis to diffusive transport for both thermalized and non-thermalized carriers. Incorporating ballistic and quasi-ballistic effects remains an important direction for future studies. Finally, model also accounts for non-radiative decay γ_{nr}, radiative recombination γ_r and Auger recombination γ_{Aug} in GaAs [66].

TABLE I. The characteristic times associated with the various ultrafast process rate underlying the two-temperature model of the GaAs material sorted in ascending order. These values are defined for electron temperatures $T_e = 300 - 10^4$ K and high-density electron-hole plasma $N_e = 10^{20}$ cm^{-3} taking into account the characteristic nonuniformity length scale $d \approx 1$ μm. Here, electron-phonon scattering rates are $\Gamma^{T_e}(N_e) = G_{\mathrm{e-ph}}(N_e)/C_e(N_e)$ and $\Gamma^{T_{ph}}(N_e, T_{ph}) = G_{\mathrm{e-ph}}(N_e)/C_{ph}(T_{ph})$. These two rates differ due to the contrast in electron and phonon heat capacities, not due to distinct scattering mechanisms. The electron-lattice thermalization is thus governed by the total rate of the electron-phonon scattering process, $\Gamma^{T_e} + \Gamma^{T_{ph}}$, corresponding to a characteristic time $\tau_{e-ph} \sim 500$ fs. The diffusion of electron concentration can be characterized by the concentration diffusion time $\tau_{\mathrm{diff}}^{N_e} = \frac{d^2}{4\pi^2 D}$, while the heat diffusion coefficients for electrons and phonons are defined as $\tau_{\mathrm{diff}}^{T_{e/ph}} = \frac{d^2}{4\pi^2 D_{e/ph}}$, where $D_{e/ph} = k_{e/ph}/C_{e/ph}$ [67] (See more details in Supplemental Information [48] Sec. 1).

Effect	Characteristic time scale	Value
Thermalization of non-thermal electrons $\mathcal{U}_{\mathrm{e}}^{\mathrm{NT}}$	$\tau_e = 1/\Gamma_e(T_e)$	≈ 200 fs
Evolution of temperatures T_e and T_{ph} due to electron-phonon scattering	$\tau_{e-ph} = 1/(\Gamma^{T_e}(N_e) + \Gamma^{T_{ph}})$	≈ 500 fs
Diffusion of electron temperature T_e	$\tau_{\mathrm{diff}}^{T_e}(d, T_e)$	≈ 2 ps - 52 fs
Diffusion of electron concentration N_e	$\tau_{\mathrm{diff}}^{N_e}(d, T_e)$	≈ 13 ps - 390 fs
Energy transfer between non-thermal electrons and phonons	$1/\Gamma_{ph}(N_e)$	≈ 0.3 ns
Diffusion of phonon temperature T_{ph}	$\tau_{\mathrm{diff}}^{T_{ph}}(d)$	≈ 80 ns

All coefficients in the system are dependent on the evolving parameters, which ultimately makes this approach complex and highly self-consistent. The self-consistency is also caused by the temporal modulation of dielectric permittivity and optical properties of structures, driven by the dynamics of carriers and phonons characteristics, which in terms changes the source functions Q_{N_e} and $Q_{\mathcal{U}_e}$.

It is worth noting that the applied model represents a substantial extension of the standard two-temperature framework [68, 69], as it explicitly accounts for both non-thermalized and thermalized carriers and their coupling to the lattice [43]. Although solving the full Boltzmann equation would offer a more rigorous description [70], it would introduce unnecessary complexity without providing significant additional insight into the key ultrafast processes examined in this study.

Dielectric permittivity. We account altering of the dielectric constant of the material via two main effects: formation of free-electron gas accounted within the Drude model [71], and band-filling effect [72] related to the occupation of the states at the bottom of the conductance band (top of the valence band) with the free carriers (see more details in Supplemental Information [48] Sec. 2). Thus, the dielectric constant of has two contributions associated with the Drude model and band-filling effect:

$$\varepsilon_{\mathrm{fin}}(\mathbf{r}, t) = [(n_0 + \Delta n_{bf}(\mathbf{r}, t)) + i(k_0 + \Delta k_{bf})(\mathbf{r}, t)]^2 + ... + \Delta\varepsilon_{Dr}(\mathbf{r}, t), \quad (2)$$

where $n_0 + ik_0$ is the initial complex refractive index of GaAs [73], while the terms $\Delta n_{bf}(\mathbf{r}, t) + i\Delta k_{bf}(\mathbf{r}, t)$ and $\Delta\varepsilon_{Dr}(\mathbf{r}, t)$ represent the change of complex refractive index due to the band filling effect and the complex dielectric permittivity modulation based on Drude model, respectively. Within the model, we also assume that dielectric constant $\varepsilon(\mathbf{r}, t)$ varies in time slowly enough that we can consider the problem segregated manner and solving stationary Maxwell's equations at each time moment t. This approximation is valid for pulses of hundreds of femtosecond and optical systems with relatively low Q-factor, and self-consistent solution of Maxwell's equations along with a carrier dynamics equations may be required. However, our research indicates that accounting for this self-consistency in the context of ultrashort pulses (with femtosecond duration) is negligible, but for longer pulse duration the developed model is essential (See Sec. 4B in SI [48]).

Finally, we implemented our theoretical model within the COMSOL Multiphysics simulation package (See Sec. 3 in SI [48]) by linking Maxwell equations with diffusion equations describing carriers dynamics in a self-consistent manner. This allows us to explore the connection between the electromagnetic field distribution $\mathbf{E}(\mathbf{r}, t)$ within the semiconductor material and the evolution of the key parameters $(\mathcal{U}_{\mathrm{e}}^{\mathrm{NT}}(\mathbf{r}, t), N_{\mathrm{e}}^{\mathrm{NT}}(\mathbf{r}, t), N_{\mathrm{e}}^{\mathrm{T}}(\mathbf{r}, t), T_{\mathrm{e}}(\mathbf{r}, t), T_{\mathrm{ph}}(\mathbf{r}, t))$ resulting in the overall variation of the optical constants and change in optical properties of the photonic structure.

B. Transient grating formation in GaAs film

We applied developed theoretical model and numerical approach to describe formation of a transient diffraction grating within a GaAs film with a height of $h = 300$ nm on an Ag substrate. To achieve this, we excited the film using two 'pump' plane wave pulses with central wavelength $\lambda_{\mathrm{pump}} = 500$ nm impinging the surface at angles

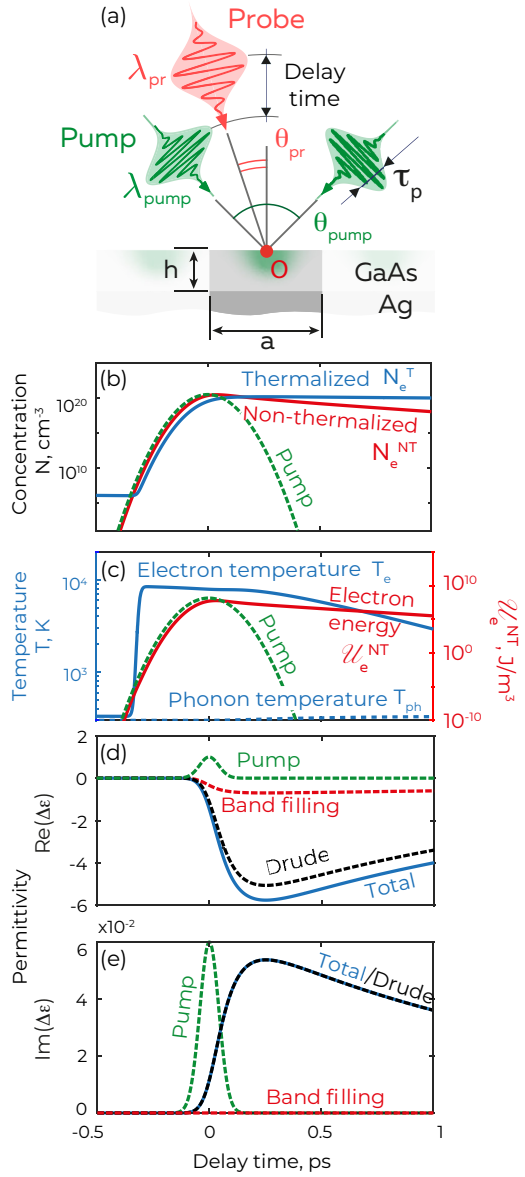

FIG. 2. (a) Interference of two pump beams forming a lattice with period a in GaAs film of height h. The dynamics of non-thermalized $N_e^{\rm NT}$ (b) and thermalized $N_e^{\rm T}$ (c) electrons concentration, energy of non-thermalized electrons $\mathcal{U}_e^{\rm NT}$ and electron temperature T_e (d) and phonon temperature T_{ph} computed at the point O in (a). b) Evolution of real (d) and imaginary (e) parts of the dielectric permittivity correspondent to the wavelength 1600 nm and computed at point O. Drude model (black dashed line) and band filling model (red dashed line) contributions are shown along with their sum ('total', blue solid line). The Gaussian pump profile is shown with a dashed green line.

$\theta_{\rm pump} = \pm 13^{\rm o}$ as shown in Fig. 2 (a). The pulse has Gaussian profile $\mathrm{GP}(t) = \mathrm{I_{pump}}\exp(-4\cdot\ln 2\cdot t^2/\tau_{\rm p}^2)$ reaching the maximal intensity about $\mathrm{I_{pump}} = 10^{14}$ W/m^2 that leads to significant evolution of the optical parameters of the film, while the pulse duration is set to $\tau_{\rm p} = 100$ fs. These pump intensity and pulse duration correspond to a fluence of F = 1 mJ/cm^2, which is below the damage threshold in GaAs [27, 74, 75]. The resulting periodical interference pattern triggers intense generation of non-equilibrium carriers. The period of this interference is a = 1100 nm corresponding to the angle of pump incidence of approximately $\theta_{\rm pump} \approx \arcsin(\lambda_{\rm pump}/(2a))$.

In Fig. 2, we plot the evolution of non-equilibrium carrier dynamics computed at one point close to the surface (point O in Fig. 2 (a)). At first, the absorbed energy of the pump pulse is transferred to the non-thermalized carriers and excite their population, causing the rapid growth of concentration N_e^{NT} (up to the values about 10^{21} cm^{-3}) and energy $\mathcal{U}_{\rm e}^{\rm NT}$ (see red solid lines in Fig. 2 (b, c)).

These hot carriers do not instantaneously attain an equilibrium energy distribution; instead, they relax via electron–electron scattering with a characteristic thermalization time $\tau_e \approx 200$ fs. As a result, after a short delay on the order of 0.2-0.3 ps, the concentration of thermalized electrons N_e^T begins to increase (see the blue solid line in Fig. 2(b)).

It reaches a maximum roughly 250 fs after the peak of the pump pulse (see Sec. 4A Fig. 4(c) in SI [48]), then subsequently decreases due to relaxation and recombination processes. This is in line with ultrafast spectroscopic studies of GaAs, which report a comparable sub-picosecond onset for carrier thermalization [76–78]. Moreover, this sub-picosecond thermalization timescale is also consistent with observations in metals, where the electron gas also thermalizes on the order of hundreds femtoseconds [79, 80].

The carrier temperature rapidly rises to values of $8\cdot 10^4 - 9\cdot 10^4$ K, reaching its peak even before the center of the excitation pulse. This phenomenon arises because the carrier heat capacity is directly proportional to their concentration in semiconductors. Consequently, the initially low heat capacity causes a rapid rise in electron temperature. Subsequently, the carrier temperature approaches a quasi-equilibrium value during the pulse and gradually decreases after the pulse ends, primarily due to electron–phonon interactions (see blue solid line in Fig. 2(c)). At the same time, the phonon temperature increases by less than 100 K over the same timescale (see blue dashed line in Fig. 2(c)). A more detailed analysis can be found in Sec. 4A in SI [48].

Finally, the predicted increase of free carrier concentration results in a drastic change of the complex dielectric permittivity Re $\varepsilon_{\rm pr} + i$Im $\varepsilon_{\rm pr}$ at the probe wavelength $\lambda_{\rm pr} = 1600$ nm as shown in FigS. 2(d) and 2(e). At the first stage, non-thermalized electrons are generated immediately after the pump pulse arrival. These electrons subsequently undergo thermalization and diffusion, leading to a corresponding modulation of the dielectric constant. One can see that at the current pump intensity, the real part of the permittivity can be reduced for 4-6 units at time scale of 1 ps which constitute almost 50% of the non-perturbed dielectric constant $\varepsilon^0 = 11.4 + i0$ [73].

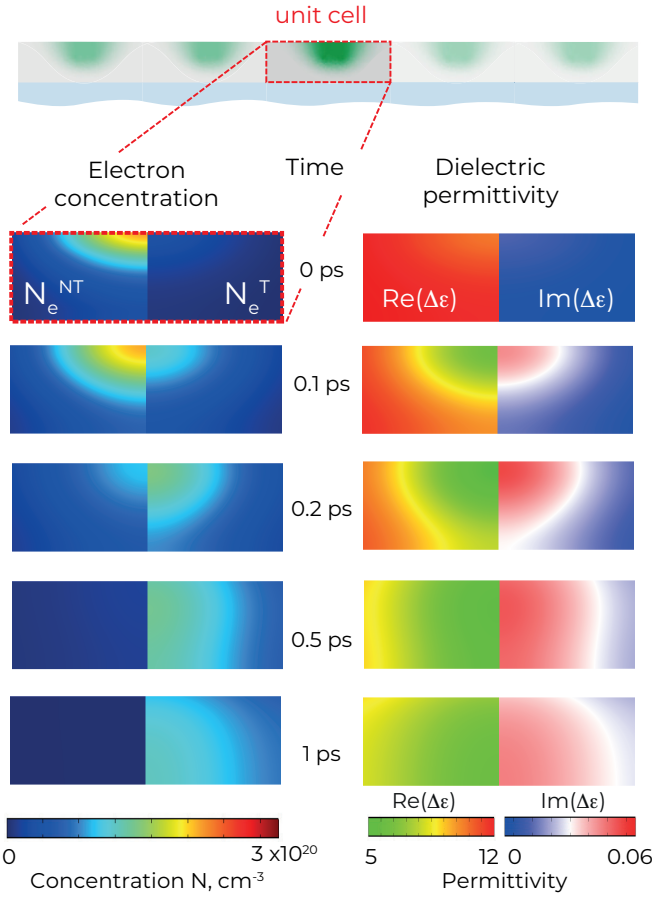

FIG. 3. The distribution of thermalized and non-thermalized electrons concentrations (left column) and real and imaginary parts of dieletric permittivity (right column) for probe wavelength $\lambda_{\rm pr} = 1600$ nm within the unit cell in GaAs film at different delay time.

This variation is predominantly provided by the Drude contribution, while the band filling component is relatively small. The increase in the imaginary part of the permittivity is clearly related to generation of free-carriers, as the impact of the band filling effect is zero for the probe wavelength of 1600 nm, which is higher than the band gap wavelength. At the same time, above the band gap, at the pump wavelength $\lambda_{\rm pump} = 500$ nm for instance, both the Drude model and the band filling effect play a substantial role in modulating the dielectric constant of the material (see Sec. 2C in SI [48]).

While previous simulations show the evolution of dielectric permittivity in time at the given point close to the film interface (point O in Fig. 2 (a)), it is quite insightful to trace the spatial distribution of generated free carriers and corresponding variation of the dielectric permittivity. The left column in Fig. 3 depicts the spatial distribution of the free carriers in a unit cell of the film at different time delays from 0 to 1 ps. One can that the initially formed non-thermalized electrons are fully converted to thermalized electrons within 0.2 ps at the depth of around $h/2 = 150$ nm, since the thermalization time $\tau_e \approx 200$ fs (See Table I). The thermalized electrons undergo the following diffusion in the depth of the film. The variation of the real and imaginary part of the dielectric permittivity (right column in Fig. 3) generally follows the free-carriers concentration forming an optical grating with high contrast. One can also notice that already at 1 ps delay the optical grating is almost vanished. Indeed, the grating contrast is defined by the inhomogeneity of the hot carriers distribution, at the same time within 1 ps the hot carriers become homogeneously distributed across the film driven by diffusion processes (See Table I). Note, that the dielectric permittivity of the film is far from the equilibrium ($\mathrm{Re}\,\varepsilon \approx 5$) and it will be kept at this values on the timescale of free carrier recombination, around 5-10 ns. Thus, the lifetime of grating is much faster than the life time of free carriers and is defined by the carrier diffusion time $\tau_{\rm diff}^{N_e}$ (See Table I).

C. Excitation of SPPs

The optically-induced diffraction grating formed within the GaAs film at picosecond timescale enables the ultrafast excitation of SPPs at the semiconductor/metal interface. As it is widely recognized, SPPs are tightly confined TM electromagnetic surface waves propagating along a metal-semiconductor interface with spectrum lying below the light cone [46]. Therefore, the induced diffraction grating ensures the quasi-phasematching condition and fulfills the quasi-wavevector conservation law, necessary for exciting SPPs from free space [81] as shown in Fig. 1:

$$\frac{2\pi}{a} + k_{\rm pr}\sin(\theta_{\rm pr}) = k_{SPP}(\omega_{\rm pr}). \qquad (3)$$

Here, $k_{\rm pr} = \omega_{\rm pr}/c$ is the wavevector of the incident probe, $\omega_{\rm pr}$ is the probe frequency, c is the speed of light, $k_{SPP}(\omega_{\rm pr})$ is the dispersion relation of SPP at the probe frequency.

The excitation of SPPs can be observed in the reflectance spectra of the probe beam. For that we plotted the reflectance amplitude as function of the probe wavelength and incidence angle shown in Fig. 4 (a) at time delay of $t_{\rm pr} = 0.2$ ps after the pump pulse arrival. One can see a distinct dip in the reflectance amplitude corresponding to the excitation of SPP. The SPP dispersion according to Eq.(3) is shown with a red dashed line for the time delay $t_{\rm pr} = 0.2$ ps. This time corresponds to the point of maximum variation in the real part of the dielectric permittivity $\Delta\mathrm{Re}\,\varepsilon_{\rm pr}$, as depicted in Fig. 3.

The distribution of H_z field component for a fixed probe wavelength $\lambda_{\rm pr} = 1600$ nm and angle $\theta_{\rm pr} = 21.3^{\rm o}$ related to the point A in Fig. 4(a) is shown in Fig. 4(b) with a clear signature of SPP mode. The temporal evolution of the reflectance amplitude for the same parameters of the probe wavelength and angle is shown in Fig. 4(c)

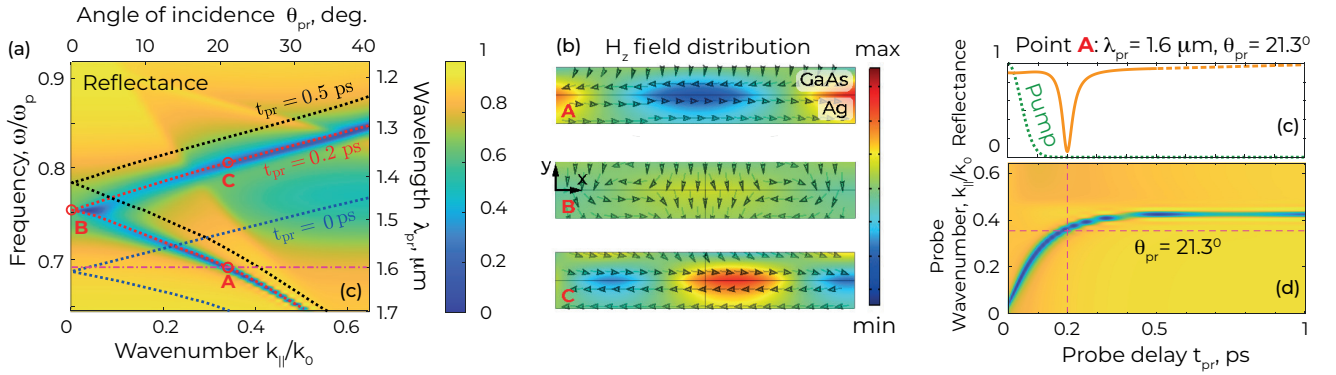

FIG. 4. (a) Reflectance map for the probe irradiation as a function of probe wavelength $\lambda_{\rm pr}$ and angle of incidence $\theta_{\rm pr}$ (frequency $\omega/\omega_p = a/\lambda_{\rm pr}$ and lateral wavenumber $k_{||}/k_0 = \sin(\theta_{\rm pr})$). The map corresponds to a fixed probe time $t_{\rm pr} = 0.2$ ps. The evolution of SPP dispersion over probe time is demonstrated through dashed lines for probe delay time $t_{\rm pr} = 0, 0.2, 0.5$ ps. (b) The magnetic field distribution H_z near the GaAs/Ag interface at a probe delay time $t_{\rm pr} = 0.2$ ps for three specific excitation points labeled as A, B, and C in Fig. 4 (a)). The arrows indicate the direction of Poynting vector. (c) The reflectance dynamics for point A ($\lambda_{\rm pr} = 1600$ nm and $q_{\rm pr} = 21.3^o$). The Gaussian pump profile is shown with a dashed green line. (d) Reflectance map of the probe beam as a function of probe delay time $t_{\rm pr}$ and normalized wavenumber $k_{||}/k_0$ for fixed probe wavelength $\lambda_{\rm pr} = 1600$ nm.

demonstrating ultrafast excitation of SPP with FWHM about 40 femtoseconds reaching almost zero reflectance. It is worth mentioning that nearly total reduction in reflectance was achieved by adjusting the film thickness of the GaAs film h under fixed pump and probe irradiation conditions ensuring the critical coupling regime. Additionally, at the same angle of incidence $\theta_{\rm pr} = 21.3^o$ and probe wavelength $\lambda_{\rm pr} = 1360$ nm (point C) it is feasible to achieve SPP excitation propagating in the opposite direction along the metal-semiconductor interface. The reverse propagation of SPP is indicated by the Pointing vector orientation depicted by arrows in Fig. 4(b) illustrating the energy flow along the interface of the structure. This figure also illustrates the magnetic field distribution H_z at normal incidence of the probing field (point B). The latter relates to the excitation of two oppositely directed SPPs, leading to the formation of a standing SPP wave.

Finally, in Fig. 4(d), we observe that the evolution of the diffraction grating, driven by the diffusion and recombination of induced nonequilibrium carriers in the conduction band (Fig. 3), causes a shift in the dispersion of the surface plasmon polariton towards shorter wavelength (see in more detail in Supplemental Information [48] Sec. 4C).

This phenomenon opens up an unprecedented way for the ultrafast control over SPPs. Actually, when operating at a fixed wavelength $\lambda_{\rm pr}$ (for example, 1600 nm) and suitable angle of incidence $\theta_{\rm pr}$ (21.3°), the phase matching with SPP is only permitted over the extremely short temporal window at around the intersection between horizontal and vertical dashed lines in Fig. 4(d). These reflectivity dynamics are computed assuming an idealized, instantaneous probe pulse. In a realistic pump–probe measurement, finite probe duration broadens ultrafast features. However, as shown in Supplemental Information [48] Fig. S6, a probe pulses of 50-100 fs duration are sufficient to resolve the sub-50 fs reflectivity dip with minimal distortion.

Moreover, while our model primarily focuses on ultrafast changes in dielectric permittivity and the resulting reflectivity modulation driven by electronic excitation, thermalization, and relaxation, coherent phonons may introduce oscillatory features in transient reflectivity through mechanisms such as band renormalization or electro-optic coupling [82, 83]. However, their overall contribution to the dielectric response is substantially smaller than that of carrier-induced effects, particularly at the high excitation densities considered in this study. Previous reports indicate that reflectivity changes due to coherent phonons are typically on the order of $1-2\%$. In contrast, our model predicts reflectivity modulation exceeding 90% ($\Delta R/R \approx 0.9$), corresponding to changes in the real part of the dielectric permittivity by approximately 6-7 units. Therefore, to model reflectivity dynamics and heat transport on picosecond timescales, we treat the lattice response as predominantly diffusive and incoherent.

III. CONCLUSION

We theoretically proposed a setup for the ultrafast generation of SPP waves at semiconductor film/metal interface by optically induced grating structure. The grating formed in a thin film of GaAs material is induced by the non-equilibrium carriers and exists at the timescales of carriers diffusion that opens an opportunity for ultrafast control over SPP below the picosecond time scale. Our results are based on a developed extended two-temperature self-consistent model that describes the ultrafast optically induced processes in GaAs film and

semiconductors in general. In particular, it demonstrates that the optimal delay between the pump pulse generating the grating and the probe pulse exciting the SPP wave, as well as the optimal angle of probe pulse incidence, are fully defined by the carriers' dynamics and can be chosen in a wide range. Finally, we believe that our advanced theoretical framework concerning ultrafast semiconductor responses to pulsed electromagnetic radiation and proposed novel technique for ultrafast SSP control exhibit significant potential for diverse applications in all-optically controlled ultrafast devices.

IV. SUPPORTING INFORMATION

The Supporting Information is available free of charge at https://pubs.acs.org.

This section provides additional details on the theoretical model and numerical simulations that describe the interaction of ultrafast semiconductor structures with pulsed laser radiation. It also includes additional information on the optically induced diffraction grating that facilitates the excitation of surface plasmon polaritons (SPPs).

V. ACKNOWLEDGEMENT

The authors are thankful Yonatan Sivan and Zarina Sadrieva for fruitful discussions. The work is funded by Russian Science Foundation and St. Peterburg Science Foundation, project №№ 25-22-20034. G.D.V. acknowledges the support from the PRIN 2022 MUR program funded by the European Union– Next Generation EU -"PNRR - M4C2, investimento 1.1 - "Fondo PRIN 2022" - HOT-carrier METasurfaces for Advanced photonics (HOTMETA), contract no. 2022LENW33 - CUP: D53D2300229 0006".

VI. REFERENCES

[1] A. I. Kuznetsov, A. E. Miroshnichenko, M. L. Brongersma, Y. S. Kivshar, and B. Luk'yanchuk, Optically resonant dielectric nanostructures, Science **354**, aag2472 (2016).

[2] Y. Kivshar, All-dielectric meta-optics and non-linear nanophotonics, National Science Review **5**, 144 (2018).

[3] K. Koshelev, S. Kruk, E. Melik-Gaykazyan, J.-H. Choi, A. Bogdanov, H.-G. Park, and Y. Kivshar, Subwavelength dielectric resonators for nonlinear nanophotonics, Science **367**, 288 (2020).

[4] D. Smirnova and Y. S. Kivshar, Multipolar nonlinear nanophotonics, Optica **3**, 1241 (2016).

[5] G. Grinblat, Nonlinear dielectric nanoantennas and metasurfaces, ACS Photonics **8**, 3406 (2021).

[6] E. A. A. Pogna, M. Celebrano, A. Mazzanti, L. Ghirardini, L. Carletti, G. Marino, A. Schirato, D. Viola, P. Laporta, C. De Angelis, and others, Ultrafast, all optically reconfigurable nonlinear nanoantenna, ACS Nano **15**, 11150 (2021).

[7] S. Makarov, S. Kudryashov, I. Mukhin, A. Mozharov, V. Milichko, A. Krasnok, and P. Belov, Tuning of magnetic optical response in a dielectric nanoparticle, Nano Letters **15**, 6187 (2015).

[8] M. Maiuri, A. Schirato, G. Cerullo, and G. Della Valle, Ultrafast all-optical metasurfaces, ACS Photonics **11**, 2888 (2024).

[9] M. R. Shcherbakov, S. Liu, V. V. Zubyuk, A. Vaskin, P. P. Vabishchevich, G. Keeler, T. Pertsch, T. V. Dolgova, I. Staude, I. Brener, and others, Ultrafast all-optical tuning of direct-gap semiconductor metasurfaces, Nature Communications **8**, 1 (2017).

[10] I. S. Sinev, K. Koshelev, Z. Liu, A. Rudenko, K. Ladutenko, A. Shcherbakov, Z. Sadrieva, M. Baranov, T. Itina, J. Liu, and others, Observation of ultrafast self-action effects in quasi-BIC metasurfaces, Nano Letters **21**, 8848 (2021).

[11] M. R. Shcherbakov, P. P. Vabishchevich, A. S. Shorokhov, K. E. Chong, D.-Y. Choi, I. Staude, A. E. Miroshnichenko, D. N. Neshev, A. A. Fedyanin, and Y. S. Kivshar, Ultrafast all-optical switching, Nano Letters **15**, 6985 (2015).

[12] Z. Zheng, D. Rocco, H. Ren, O. Sergaeva, Y. Zhang, K. B. Whaley, C. Ying, D. de Ceglia, C. De-Angelis, M. Rahmani, and others, Advances in nonlinear metasurfaces, Nanophotonics **12**, 4255 (2023).

[13] S. Gennaro, R. Sarma, and I. Brener, Nonlinear and ultrafast all-dielectric metasurfaces, Nanotechnology **33**, 402001 (2022).

[14] Z. Yang, M. Liu, D. Smirnova, A. Komar, M. Shcherbakov, T. Pertsch, and D. Neshev, Ultrafast q-boosting in semiconductor metasurfaces, Nanophotonics **13**, 2173 (2024).

[15] G. Della Valle, B. Hopkins, L. Ganzer, T. Stoll, M. Rahmani, S. Longhi, Y. S. Kivshar, C. De Angelis, D. N. Neshev, and G. Cerullo, Nonlinear anisotropic dielectric metasurfaces, ACS Photonics **4**, 2129 (2017).

[16] D. A. Shilkin, S. T. Ha, R. Paniagua-Domínguez, and A. I. Kuznetsov, Ultrafast modulation of a nonlocal semiconductor metasurface, Nano Letters **2024**, 1 (2024).

[17] M. Celebrano, D. Rocco, M. Gandolfi, A. Zilli, F. Rusconi, A. Tognazzi, A. Mazzanti, L. Ghirardini, E. A. Pogna, L. Carletti, and others, Optical tuning of dielectric nanoantennas, Optics Letters **46**, 2453 (2021).

[18] D. Rocco, M. Gandolfi, A. Tognazzi, O. Pashina, G. Zograf, K. Frizyuk, C. Gigli, G. Leo, S. Makarov, M. Petrov, and others, Opto-thermally controlled beam steering, Optics Express **29**, 37128 (2021).

[19] T. V. Tsoulos and G. Tagliabue, Self-induced thermo-optical effects, Nanophotonics **9**, 3849 (2020).

[20] M. Rahmani, L. Xu, A. E. Miroshnichenko, A. Komar, R. Camacho-Morales, H. Chen, Y. Zárate, S. Kruk, G. Zhang, D. N. Neshev, and others, Reversible thermal tun-

ing of metasurfaces, Advanced Functional Materials **27**, 1700580 (2017).
[21] T. Zhang, Y. Che, K. Chen, J. Xu, Y. Xu, T. Wen, G. Lu, X. Liu, B. Wang, X. Xu, and others, Anapole mediated giant photothermal nonlinearity in nanostructured silicon, Nature Communications **11**, 3027 (2020).
[22] Y.-S. Duh, Y. Nagasaki, Y.-L. Tang, P.-H. Wu, H.-Y. Cheng, T.-H. Yen, H.-X. Ding, K. Nishida, I. Hotta, J.-H. Yang, and others, Giant photothermal nonlinearity in a single silicon nanostructure, Nature Communications **11**, 4101 (2020).
[23] K. Nishida, P.-H. Tseng, Y.-C. Chen, P.-H. Wu, C.-Y. Yang, J.-H. Yang, W.-R. Chen, O. Pashina, M. I. Petrov, K.-P. Chen, and others, Optical bistability in nanosilicon with record low Q-factor, Nano Letters **23**, 11727 (2023).
[24] G. P. Zograf, M. I. Petrov, S. V. Makarov, and Y. S. Kivshar, All-dielectric thermonanophotonics, Advances in Optics and Photonics **13**, 643 (2021).
[25] D. Ryabov, O. Pashina, G. Zograf, S. Makarov, and M. Petrov, Nonlinear optical heating of all-dielectric supercavity, Nanophotonics **11**, 3981 (2022).
[26] C. Husko and C. W. Wong, Ultrafast all-optical bistability in AlGaAs photonic crystals, Proc. SPIE **6393**, 111 (2006).
[27] A. Di Cicco, G. Polzoni, R. Gunnella, A. Trapananti, M. Minicucci, S. Rezvani, D. Catone, L. Di Mario, J. Pelli Cresi, S. Turchini, and others, Broadband optical ultrafast reflectivity of Si, Ge and GaAs, Scientific Reports **10**, 17363 (2020).
[28] G. Crotti, M. Akturk, A. Schirato, V. Vinel, A. A. Trifonov, I. C. Buchvarov, D. N. Neshev, R. Proietti Zaccaria, P. Laporta, A. Lemaitre, and others, Giant ultrafast dichroism and birefringence, Light: Science & Applications **13**, 204 (2024).
[29] A. Tognazzi, P. Franceschini, O. Sergaeva, L. Carletti, I. Alessandri, G. Finco, O. Takayama, R. Malureanu, A. V. Lavrinenko, A. C. Cino, and others, Giant photoinduced reflectivity modulation, Advanced Photonics **5**, 066006 (2023).
[30] Y. Yang, W. Wang, A. Boulesbaa, I. I. Kravchenko, D. P. Briggs, A. Puretzky, D. Geohegan, and J. Valentine, Nonlinear Fano-resonant dielectric metasurfaces, Nano Letters **15**, 7388 (2015).
[31] M. A. Masharin, T. Oskolkova, F. Isik, H. Volkan Demir, A. K. Samusev, and S. V. Makarov, Giant ultrafast all-optical modulation based on exceptional points, ACS Nano **18**, 3447 (2024).
[32] R. Berté, T. Possmayer, A. Tittl, L. d. S. Menezes, and S. A. Maier, Emergent resonances in a thin film tailored by optically-induced small-permittivity asymmetries, arXiv:2403.05730 (2024).
[33] I. Staude, T. Pertsch, and Y. S. Kivshar, All-dielectric resonant meta-optics lightens up, ACS Photonics **6**, 802 (2019).
[34] D. Pennington and C. Harris, Dynamics of photothermal surface expansion and diffusivity using laser-induced holographic gratings, IEEE Journal of Quantum Electronics **28**, 2523 (1992).
[35] O. Käding, H. Skurk, A. Maznev, and E. Matthias, Transient thermal gratings at surfaces for thermal characterization, Applied Physics A **61**, 253 (1995).
[36] K. Chen, N. Sheehan, F. He, X. Meng, S. C. Mason, S. R. Bank, and Y. Wang, Measurement of ambipolar diffusion coefficient, ACS Photonics **4**, 1440 (2017).
[37] C. Hoffman, K. Jarašiūnas, H. Gerritsen, and A. Nurmikko, Measurement of surface recombination via transient gratings, Applied Physics Letters **33**, 536 (1978).
[38] T. Sjodin, C.-M. Li, H. Petek, and H.-L. Dai, Ultrafast transient grating scattering studies of carrier dynamics, Chemical Physics **251**, 205 (2000).
[39] N. Gouaichault, J. Iehl, R. Grac, M. Pugnet, and J. Collet, Picosecond transient gratings in GaAs: experiments and modelling, Optical Materials **4**, 262 (1995).
[40] W. Marine and P. Mathiez, Dynamics of laser annealing of amorphous Ge and GaAs films using transient gratings, IEEE Journal of Quantum Electronics **22**, 1404 (1986).
[41] L. Gomez-Jahn and R. D. Miller, Picosecond surface-restricted transient grating studies, Journal of Chemical Physics **96**, 3981 (1992).
[42] Y. Yang, N. Kamaraju, S. Campione, S. Liu, J. L. Reno, M. B. Sinclair, R. P. Prasankumar, and I. Brener, Transient GaAs plasmonic metasurfaces at terahertz frequencies, ACS Photonics **4**, 15 (2017).
[43] Y. Sivan and M. Spector, Ultrafast dynamics of optically induced heat gratings in metals, ACS Photonics **7**, 1271 (2020).
[44] A. Schirato, M. Maiuri, A. Toma, S. Fugattini, R. Proietti Zaccaria, P. Laporta, P. Nordlander, G. Cerullo, A. Alabastri, and G. Della Valle, Transient optical symmetry breaking for ultrafast broadband dichroism in plasmonic metasurfaces, Nature Photonics **14**, 723 (2020).
[45] A. Schirato, G. Crotti, R. Proietti Zaccaria, A. Alabastri, and G. Della Valle, Hot carrier spatio-temporal inhomogeneities in ultrafast nanophotonics, New Journal of Physics **24**, 045001 (2022).
[46] L. Zheng, U. Zywietz, A. Evlyukhin, B. Roth, L. Overmeyer, and C. Reinhardt, Experimental demonstration of surface plasmon polariton reflection and transmission effects, Sensors **19**, 4633 (2019).
[47] Y. Dubi and Y. Sivan, "Hot" electrons in metallic nanostructures — non-thermal carriers or heating?, Light: Science & Applications **8**, 89 (2019).
[48] See Supplemental Material at [URL will be inserted by publisher] (including references [49-57]) for additional details on the theoretical model, numerical simulations, and the optically induced transient grating enabling SPP excitation.
[49] L. Shi, K. Xu, and L.-W. Wang, Comparative study of ab initio nonradiative recombination rate calculations under different formalisms, Phys. Rev. B **91**, 205315 (2015).
[50] H. Ito and T. Ishibashi, Surface Recombination Velocity in p-Type GaAs, Jpn. J. Appl. Phys. **33**, 88 (1994).
[51] D. Steiauf, E. Kioupakis, and C. G. Van de Walle, Auger Recombination in GaAs from First Principles, ACS Photonics **1**, 643 (2014).
[52] M. Neuhaus et al., Transient field-resolved reflectometry at 50–100 THz, Optica **9**, 42 (2022).
[53] T. C. Phong, N. D. Hien et al., Comparison of electron scattering by acoustic-phonons in two types of quantum wells with GaAs and GaN materials, Nanoscale Adv. **6**, 832 (2024).
[54] N. G. Nilsson, Empirical approximations for the Fermi energy in a semiconductor with parabolic bands, Appl. Phys. Lett. **33**, 653 (1978).
[55] M. D. Sturge, Optical absorption of gallium arsenide between 0.6 and 2.75 eV, Phys. Rev. **129**, 2835 (1963).
[56] Silver, Ag, (2023), [Online; accessed 8 Nov 2023].

[57] M. Pokorny and Z. Raida, Transmission Line on Semiconductor Substrate with Distributed Amplification, Radioengineering **19**, 1 (2010).

[58] K. Oguri, T. Tsunoi, K. Kato, H. Nakano, T. Nishikawa, K. Tateno, T. Sogawa, and H. Gotoh, Dynamical observation of photo-Dember effect on semi-insulating GaAs, Applied Physics Express **8**, 022401 (2015).

[59] B. Schumann, Properties of Gallium Arsenide, Cryst. Res. Technol. **26**, 18 (1991).

[60] T. J.-Y. Derrien, T. Sarnet, M. Sentis, and T. E. Itina, Application of a two-temperature model for femtosecond-laser-induced structures on Si, J. Optoelectron. Adv. Mater. **12**, 610 (2011).

[61] Ioffe Institute, Physical properties of Gallium Arsenide (GaAs), online resource (2001).

[62] R. A. Höpfel, J. Shah, P. A. Wolff, and A. C. Gossard, Electron-hole scattering in GaAs quantum wells, Phys. Rev. B **37**, 6941 (1988).

[63] A. Margiolakis, G. D. Tsibidis, K. M. Dani, and G. P. Tsironis, Ultrafast dynamics and subwavelength structure formation in GaAs, Phys. Rev. B **98**, 224103 (2018).

[64] B. A. Ruzicka, L. K. Werake, H. Samassekou, and H. Zhao, Ambipolar diffusion of photoexcited carriers in bulk GaAs, Applied Physics Letters **97**, 1 (2010).

[65] M. Heiblum, M. Nathan, D. C. Thomas, and C. Knoedler, Direct observation of ballistic transport in GaAs, Physical Review Letters **55**, 2200 (1985).

[66] U. Strauss, W. W. Rühle, and K. Köhler, Auger recombination in intrinsic GaAs, Applied Physics Letters **62**, 55 (1993).

[67] A. Block, M. Liebel, R. Yu, M. Spector, Y. Sivan, F. García de Abajo, and N. F. van Hulst, Tracking ultrafast hot-electron diffusion in space and time, Science Advances **5**, eaav8965 (2019).

[68] B. H. Christensen, K. Vestentoft, and P. Balling, Short-pulse ablation rates and the two-temperature model, Applied Surface Science **253**, 6347 (2007).

[69] A. Schirato, G. Crotti, R. Proietti Zaccaria, A. Alabastri, and G. Della Valle, Hot carrier spatio-temporal inhomogeneities in ultrafast nanophotonics, New Journal of Physics **24**, 045001 (2022).

[70] N. Del Fatti, C. Voisin, M. Achermann, S. Tzortzakis, D. Christofilos, and F. Vallée, Nonequilibrium electron dynamics in noble metals, Physical Review B **61**, 16956 (2000).

[71] K. Sokolowski-Tinten and D. von der Linde, Generation of dense electron-hole plasmas in silicon, Phys. Rev. B **61**, 2643 (2000).

[72] B. Bennett, R. Soref, and J. Alamo, Carrier-induced refractive index change in InP, GaAs and InGaAsP, IEEE Journal of Quantum Electronics **26**, 113 (1990).

[73] K. Papatryfonos, T. Angelova, A. Brimont, B. Reid, S. Guldin, P. Smith, M. Tang, K. Li, A. Seeds, H. Liu, and D. Selviah, Refractive indices of MBE-grown $Al_xGa_{1-x}As$ in the transparent region, AIP Advances **11**, 025327 (2021).

[74] E. Glezer, Y. Siegal, L. Huang, and E. Mazur, Laser-induced band-gap collapse in GaAs, Physical Review B **51**, 6959 (1995).

[75] A. P. Singh, A. Kapoor, and K. Tripathi, Ripples and grain formation in GaAs surfaces exposed to ultrashort laser pulses, Optics & Laser Technology **34**, 533 (2002).

[76] P. M. Fauchet, T. Gong, P. J. Kelly, and J. F. Young, Femtosecond gain dynamics in thin GaAs films, Semiconductor Science and Technology **7**, B164 (1992).

[77] B. Ziaja, N. Medvedev, V. Tkachenko, T. Maltezopoulos, and W. Wurth, Time-resolved observation of band-gap shrinking and electron-lattice thermalization in X-ray excited GaAs, Scientific Reports **5**, 18068 (2015).

[78] H. Tanimura, K. Tanimura, and J. Kanasaki, Ultrafast relaxation of photoinjected nonthermal electrons in the γ-valley of GaAs, Physical Review B **104**, 245201 (2021).

[79] C. Guo, G. Rodriguez, and A. J. Taylor, Ultrafast dynamics of electron thermalization in gold, Physical Review Letters **86**, 1638 (2001).

[80] M. Lisowski, P. Loukakos, U. Bovensiepen, J. Stähler, C. Gahl, and M. Wolf, Ultra-fast dynamics of electron thermalization, cooling and transport in Ru(001), Applied Physics A **78**, 165 (2004).

[81] G. Liang, Z. Luo, K. Liu, Y. Wang, D. Jianxiong, and Y. Duan, Fiber-optic surface plasmon resonance biosensor technique, Critical Reviews in Analytical Chemistry **46**, 0 (2015).

[82] G. C. Cho, W. Kütt, and H. Kurz, Subpicosecond time-resolved coherent-phonon oscillations in GaAs, Physical Review Letters **65**, 764 (1990).

[83] P. Ruello and V. E. Gusev, Physical mechanisms of coherent acoustic phonon generation by ultrafast laser excitation, Ultrasonics **56**, 21 (2015).